MSc in Photonics

Universitat Politècnica de Catalunya (UPC)
Universitat Autònoma de Barcelona (UAB)
Universitat de Barcelona (UB)
Institut de Ciències Fotòniques (ICFO)

http://www.photonicsbcn.eu

PHOTONICS**BCN**

Master in Photonics

MASTER THESIS WORK

OPTICAL SIMULATOR OF TWO ATOMS IN A DOUBLE WELL

Arnau Fabra Ruiz

Supervised by Dr./Prof. Maciej Lewenstein (ICFO) and Dr. Miguel Ángel Garcia-March (ICFO)

Presented on date 9th September 2019

Registered at

Escola Tècnica Superior d'Enginyeria de Telecomunicació de Barcelona

Optical simulator of two atoms in a double well

Arnau Fabra Ruiz

ICFO - The Institute of Photonic Sciences, Mediterranean Technology Park, Castelldefels (Barcelona), Catalonia, Spain

E-mail: arnau.fabra@gmail.com

Abstract. We show that optical fibers with an inhomogeneous refractive index profile and thin metallic slabs can be used to simulate a one dimensional system of two interacting particles in a double well. We first study the single particle energies. We use them to characterize the states at the limit of infinitely high interacting barrier. The states are classified by their symmetries. We demonstrate that the optical system is able to produce wave chaos which is analogous of quantum chaos in our simulated system, that is, the spacing between the energy levels follows the Wigner-Dyson distribution. We prove these results with two different methods, corresponding to first and second quantization in the simulated atom systems.

1. Introduction

The cognitive process of acquiring information from a particular object by comparing it to another is called analogy. In this report we set an analogy between a graded index (GRIN) optical fiber with three thin slabs of metallic materials with specific positions (see figure 1b), and a quantum system of two atoms interacting in a double well (DW) (see figure 1a). GRIN fibers represent the perfect environment for this situation because its refractive index decreases continously from the center of the fiber to the edges [1]. To this end, we consider the paraxial propagation of a polarized monochromatic laser beam in such a fiber. Then, the propagation equation is analogue to the Schrödinger equation. The longitudinal dimension along the fiber plays the role of the time in our quantum system, while the inhomogeneous refractive index profile of the fiber plays the role of external interaction potentials. In our analogy, the GRIN modulation of the refractive index is analogous to a parabolic trap potential for the two atoms, two of the metallic slabs play the role of the central barrier of the DW and another metallic slab plays the role of the contact interactions. This model is an example of an analogy between a classical and a quantum system, in particular, it is a quantum-optical analogy, which benefits from the wave aspect in both fields [2].

One of the most significant parameters to study in this kind of few-atom systems is the symmetry [3]. Here it is used to determine whether the states are fermionic or bosonic. Indeed, in some cases this kind of symmetry is used to study the boson states when only

fermion ones are available, by means of the Bose-Fermi mapping theorem [4].
One-dimensional quantum systems have been the spotlight of many theorists due to the existence of exact solutions and manageable numeric calculations [5]. Many of them centered their studies either on energies [6] or correlations [7]. In this report we perform a study of energies and states from numerical calculations (for more examples see [8]).
Nowadays, the notion of quantum chaos is used in a very broad context [9, 10]. Quantum chaos is associated with level repulsion and highly delocalized eigenstates, and that is what is studied in this report [11]. What we find in our classical system is wave chaos, which is analogous of quantum chaos in our simulated system [12].
This thesis is organized as follows. In section 2 we detail the characteristics of the fiber under study. We build the analogy with the quantum system in section 3, where we also derive the equations in second quantization. In section 4 we discuss the energy levels and the different states of our system, its properties and symmetries. In section 5 we do the quantum chaos study and discuss the final results. The conclusions are explained in section 6.

2. Optical system: grin fiber with three thin metallic slabs

The paraxial propagation of a monochromatic optical beam of constant polarization along an optical fiber with an inhomogeneous refractive index profile is given by

$$-2\,i\,n_0\,k_0\frac{\partial}{\partial\tilde{z}}\tilde{\Phi}=\left[\nabla_t^2+k_0\left(\tilde{n}^2(\tilde{x},\tilde{y})-n_0^2\right)\right]\tilde{\Phi}, \tag{1}$$

where ∇_t^2 is the Laplacian in the transverse coordinates, $\tilde{n}^2(\tilde{x},\tilde{y})$ is the index of refraction profile with a reference value n_0, k_0 is the wavenumber, $\tilde{z}$ is the axial coordinate of the fiber and x, y are the transverse coordinates. To perform a comparison to the Schrödinger equation, we divide by $-2n_0k_0$, in such a way the length units are removed

$$i\frac{\partial}{\partial z}\Phi=\left(-\frac{1}{2}\nabla_{x,y}^2+\Delta n(x,y)\right)\Phi, \tag{2}$$

where we have the dimensionless coordinates $x=k_0\sqrt{n_0}\tilde{x}$, $y=k_0\sqrt{n_0}\tilde{y}$ and $z=k_0\,\tilde{z}$, we have that $\Phi(x,y,z)=\tilde{\Phi}(\tilde{x},\tilde{y},\tilde{z})$, $n(x,y)=\tilde{n}(\tilde{x},\tilde{y})$ and $\Delta n(x,y)=[n_0^2-n^2(x,y)]/2n_0$. The longitudinal and transverse coordinates can be easily separated by making the substitution $\Phi(x,y,z)=\exp(-i\mu z)\phi(x,y)$, where μ is the paraxial propagation constant. With that last definition we get an expression equivalent to solving for the energy spectrum of a quantum Hamiltonian with two degrees of freedom

$$H\phi(x,y)\equiv\left(-\frac{1}{2}\nabla_{x,y}^2+\Delta n(x,y)\right)\phi(x,y)=\mu\phi(x,y). \tag{3}$$

The paraxial equation is indeed sometimes called the optical Schrödinger equation or the Fock-Leontovich equation [13]. The effective potential for the analogy is built by combining GRIN fibers with thin metal slabs composed by two different materials. The refractive index of a GRIN fiber decreases continuously with the radial distance to the optical axis of the fiber, so we consider a particular case of a parabolic profile that focuses

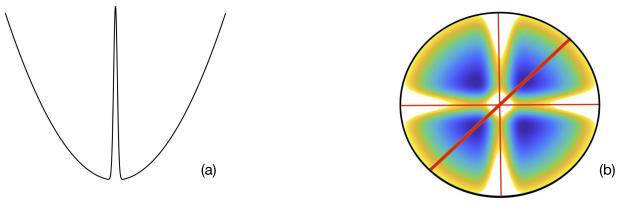

Figure 1: (a) Simulated system. (b) Schematic of the section of the fiber, the red lines represent the thin metallic slabs in our optics system and the potentials in our quantum system.

the beam and provides guidance in the fiber, what is called an harmonic potential for two dimensions:

$$\Delta n_{\rm GRIN}(x,y) = \begin{cases} \frac{1}{2}\,\omega\,(x^2+y^2), & \text{if } \rho = \sqrt{x^2+y^2} < R \\ \frac{1}{2}\,\omega\,R^2, & \text{if } \rho = \sqrt{x^2+y^2} \geq R. \end{cases} \tag{4}$$

The metal slabs are placed in very specific positions (see figure 1b). We model these slabs as thin Gaussian barriers which we add to the GRIN refractive index profile,

$$\Delta n_{\rm dw}(x,y) = \frac{V_0}{2}\exp\left(\frac{-x^2}{2\sigma_{\rm dw}^2}\right) + \frac{V_0}{2}\exp\left(\frac{-y^2}{2\sigma_{\rm dw}^2}\right), \tag{5}$$

$$\Delta n_{\rm g}(x,y) = \frac{g}{\sigma_g\sqrt{2\pi}}\exp\left(\frac{-(x-y)^2}{2\sigma_g^2}\right). \tag{6}$$

The first function $\Delta n_{\rm dw}(x,y)$ has two maxima at lines $x = 0$ and $y = 0$, while the second function $\Delta n_{\rm g}(x,y)$ has one maximum at line $x = y$. So by working with very small widths ($\sigma_{\rm dw}$, σ_g) we simulate the desired delta potential, as we discuss in next section.

The relationship of the constants V_0 in (5) and g in (6) with the optical parameters is of practical importance. So by recovering the spacial dimensions $\tilde{\sigma}_g = \sigma_g\,\lambda_g$, one obtains

$$\frac{\Delta n_{\rm dw}^{\rm max}(\lambda_{\rm dw})}{2} = V_0 \qquad \text{and} \qquad \frac{\Delta n_g^{\rm max}(\lambda_g)\,\sqrt{2\pi}\,\tilde{\sigma}_g}{\lambda_g} = g, \tag{7}$$

where the left hand sides only contain optical parameters. This means that experimentally it could be done with thin slabs of metallic materials of widths $\tilde{\sigma}_{\rm dw}$ and $\tilde{\sigma}_g$, for which $\Delta n_i^{\rm max} = (n_0^2 - n_{{\rm metal}_i})/2n_0$. Combining the thin metal slabs with the GRIN fiber we will get a total refractive index of $\Delta n_{\rm tot} = \Delta n_{\rm dw} + \Delta n_g + \Delta n_{\rm GRIN}$.

3. Optical analogy to the two-particle in a double well

To establish that the fiber simulates the two-body one-dimensional system, we first consider the quantum Hamiltonian of two particles in a one dimensional Harmonic trap [14]

$$H_0 = \frac{1}{2}\sum_{i=1}^{2}\left(-\frac{d^2}{dx_i^2} + x_i^2\right). \tag{8}$$

In order to make this simpler, we have scaled all distances by the harmonic oscillator length $a = \sqrt{\hbar/(m\omega)}$ (and taken $\hbar = \omega = 1$); in this way we can define the coordinates

x_i as the dimensionless positions of the two particles. At this point it is needed to add two-body interactions to the trap Hamiltonian, $V_g(|x_2 - x_1|)$. In this situation, we will only use the contact interactions, $V_{\rm int} = g\,\delta(x_1 - x_2)$. However, in our model this will be simulated by taking V_g as a narrow Gaussian

$$V_{\rm int} = \frac{g}{\sigma_{\rm g}\sqrt{2\pi}} \exp\left(\frac{-(x_2 - x_1)^2}{2\sigma_{\rm g}^2}\right). \tag{9}$$

The last step consist in adding the DW trap (see figure 1a)

$$V_{\rm dw} = \frac{V_0}{2} \sum_{i=1}^{2} \exp\left(\frac{-x_i^2}{2\sigma_{\rm dw}^2}\right). \tag{10}$$

So if we finally put together all the terms $H = H_0 + V_{\rm int} + V_{\rm dw}$ we recover the effective Hamiltonian whose associated Shrödinger equation is the analogous to the paraxial equation of previous section [15]. In our analogy, the coordinates x_1 and x_2 correspond to the (x, y) coordinates of the system, the refractive index $\Delta n_{\rm tot}$ will work as the potential with inverted sign and z will work as the time. The diagonal $x_1 = x_2$ represents the contact interactions and the gaussians at $x_1 = 0$ and $x_2 = 0$ represent the DW for the particle of the coordinate x_1 and x_2.

3.1. Second quantization

Here we briefly explain the approach we use to do a direct diagonalization in second quantization. In first place, we have the Hamiltonian defined with the field operators

$$H = \int \hat{\Psi}_{\rm B}^\dagger H_{\rm sp} \hat{\Psi}_{\rm B} + \frac{g}{2} \int \hat{\Psi}_{\rm B}^\dagger \hat{\Psi}_{\rm B}^\dagger \hat{\Psi}_{\rm B} \hat{\Psi}_{\rm B}, \tag{11}$$

where $H_{\rm sp} = \frac{1}{2}\frac{\partial^2}{\partial x^2} + V_{\rm DW}(x)$. Now we expand the second quantized field operators into eigenfunctions $\phi_n(x)$ of the single-particle Hamiltonian for the harmonic oscillator

$$\hat{\Psi} = \sum_{n=0}^{M} \hat{a}_n\, \phi_n(x) \qquad \text{and} \qquad \hat{\Psi}^\dagger = \sum_{n=0}^{M} \hat{a}_n^\dagger\, \phi_n^*(x), \tag{12}$$

where the creation and annihilation operators $\hat{a}_n$ and $\hat{a}_n^\dagger$ satisfy the bosonic commutation relations $[\hat{a}_i, \hat{a}_j^\dagger] = \delta_{ij}$ and $[\hat{a}_i, \hat{a}_j] = [\hat{a}_i^\dagger, \hat{a}_j^\dagger] = 0$. Here, M is the number of modes used in the expansion. The Hamiltonian can be written as

$$\hat{H} = \sum_{n=0}^{M} E_n \hat{n}_n + \frac{g}{2} \sum_{ijkl} U_{ijkl}\, \hat{a}_i^\dagger \hat{a}_j^\dagger \hat{a}_k \hat{a}_l, \tag{13}$$

where $\hat{n}_n = \hat{a}_n^\dagger \hat{a}_n$ and $U_{ijkl} = \int \phi_i^* \phi_j^* \phi_k \phi_l \,{\rm d}x$. To calculate the final matrix we have to do the brakets of all the states of the basis and to diagonalize it.

We thus perform the diagonalization in two ways: (i) in first quantization, with the gaussian approximation of the contact interactions, and (ii) in the second quantization, with contact interactions and a truncation in the number of modes.

4. Energy spectra

Now that the analogy have been established, we make a study of the energy levels of our system. In figure 2a we can see the single particle energies as a function of the V_0, the parameter that determines the height of the DW barrier. The energies when $V_0 = 0$ represent the solutions to the quantum harmonic oscillator $E_n = \hbar\omega(n + \frac{1}{2})$, when V_0 is increased we get a degeneration of the energies in pairs. The energies will be very important for the study of the total energy spectra, since the total energies will be a combination of the single particle energies.

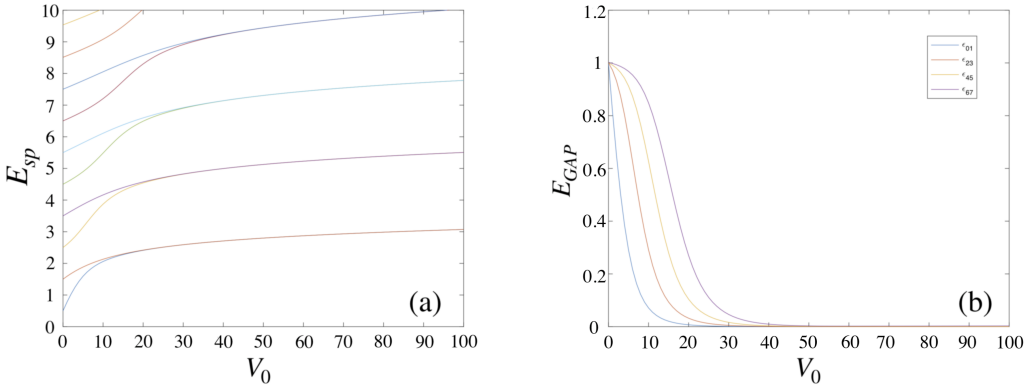

Figure 2: (a) First ten eigenvalues of the single-particle Hamiltonian as a function of V_0. (b) Energy gap of the first four pairs of single particle energies. Both graphs are calculated with the first quantization method.

To identify which total states are bosonic or fermionic we have to study the symmetry respect to the contact interactions line ($x_1 = x_2$). If the final state is symmetric, it will be bosonic; and if the final state is antisymmetric, it will be fermionic. To apply that in our first quantization numerics, we will use an operator that interchanges the positions of the two particles $x_1 \to x_2$, that will gives a $+1(-1)$ for bosonic (fermionic) states.
Now, to study the total energies of the system we need to use this last differentiation between bosons and fermions, the first ones will be affected by the interactions while the second ones will not. For the ideal case of delta interactions, when there is no interactions, both energies coincide; however, when interactions increase the bosonic energies increase and the fermionic ones remain constant, see figure 3.
We can use the fermionic states to determine the energy of the bosonic ones at $g \to \infty$. The fermionic ground state is: $\Psi_0^{\mathrm{f}}(x_1, x_2) = 1/\sqrt{2}\,\mathrm{Slater}(\phi_0, \phi_1) = 1/\sqrt{2}\,(\phi_0(x_1)\phi_1(x_2) - \phi_0(x_2)\phi_1(x_1))$, where Slater refers to the Slater determinant [4]. This state corresponds to the localization of one atom in each well and has energy $E_0 = \varepsilon_0 + \varepsilon_1$ for all g, we can easily check it by looking that if we sum the two first energies of figure 2a at $V_0 = 100$ we get exactly the ground state energy of figure 3. In the plots of figure 2, we see that the first two single particle states are quasi-degenerate, $\varepsilon_1 = \varepsilon_0 + \varepsilon_{01}$ with $\varepsilon_{01} \ll \varepsilon_0$ for $V_0 \geq 25$. The first four fermionic excited states are $\Psi_1^{\mathrm{f}} \sim \mathrm{Slater}(\phi_0, \phi_2)$, $\Psi_2^{\mathrm{f}} \sim \mathrm{Slater}(\phi_1, \phi_2)$, $\Psi_3^{\mathrm{f}} \sim \mathrm{Slater}(\phi_0, \phi_3)$ and $\Psi_4^{\mathrm{f}} \sim \mathrm{Slater}(\phi_1, \phi_3)$. Thus the energies of the first four fermionic excited states are $E_1 = \varepsilon_0 + \varepsilon_2$, $E_2 = \varepsilon_1 + \varepsilon_2 + \varepsilon_{01}$, $E_3 = \varepsilon_0 + \varepsilon_2 + \varepsilon_{23}$

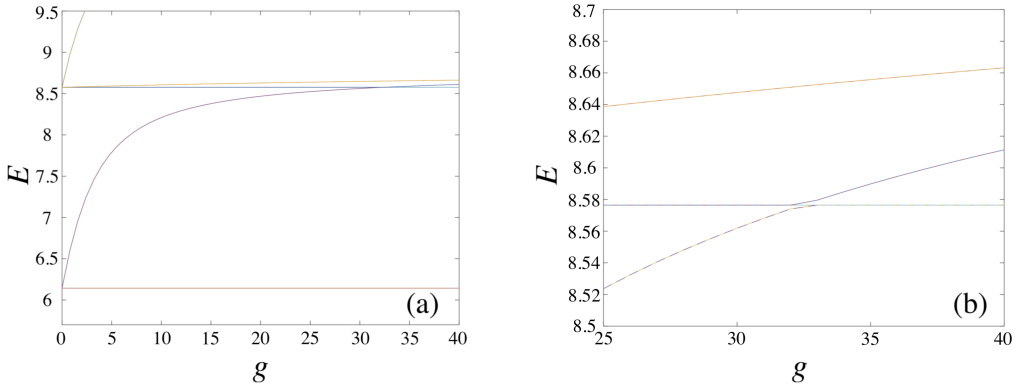

Figure 3: (a) Energy spectra as a function of the coupling constant g for $V_0 = 100$ with the first quantization method. (b) Avoided crossings section obtained from the enlargement of (a), we can see that there are more than three states thanks to the dashed lines.

and $E_4 = \varepsilon_1 + \varepsilon_2 + \varepsilon_{01} + \varepsilon_{23}$. With the plots of figure 2 again we can see that for $V_0 \geq 30$ we have that $\varepsilon_{23} \ll \varepsilon_2$, so in this regime the four energies are quasi-degenerated.
For sufficiently high DW barrier, a lot of pairs of single particle states are quasi-degenerate. It allows us to define the following wavefunctions:

$$\phi_n^j = \begin{cases} \phi_n^L = \dfrac{1}{\sqrt{2}}(\phi_{2n} + \phi_{2n+1}) \\ \phi_n^R = \dfrac{1}{\sqrt{2}}(\phi_{2n} - \phi_{2n+1}) \quad , n = 0, 1, ..., \end{cases} \tag{14}$$

where j=R(L) stands for right (left). These ϕ_n^j functions are mostly localized either in the left or right well when the pair of delocalized functions ϕ_n used to construct them are quasi-degenerate. They are eigenstates of the single particle Hamiltonian only if all quasi-degenerate states are zero, which occur for infinite barrier heights of the DW.
For a finite quasi-degeneracy between the single particle energies (and therefore to a finite barrier height), certain width of the DW or contact interactions barrier will induce such a localization of the atom at some limit [7]. Therefore, the first four fermionic excited states will resemble the states described in the previous paragraph. In other words, since our contact interactions are not a perfect delta function (they have some width), they produce a perturbation in our system that makes that our final eigenstates will be a combination of the eigenstates of the ideal system. In figure 4 we can see the states that correspond to the Slater determinants (first row) and the perturbed solutions we get (second row): $\tilde{\Psi}_1^{\mathrm{f}} = \Psi_1^{\mathrm{f}} - \Psi_4^{\mathrm{f}}$, $\tilde{\Psi}_2^{\mathrm{f}} = \Psi_3^{\mathrm{f}} - \Psi_2^{\mathrm{f}}$, $\tilde{\Psi}_3^{\mathrm{f}} = \Psi_3^{\mathrm{f}} + \Psi_2^{\mathrm{f}}$ and $\tilde{\Psi}_4^{\mathrm{f}} = \Psi_1^{\mathrm{f}} + \Psi_4^{\mathrm{f}}$. These boson perturbed states can be calculated by the symmetrization of the fermion ones if the interactions are big enough using the Bose-Fermi mapping theorem [8], or by the direct diagonalization of the total Hamiltonian, the method we have used to obtain the third row of figure 4. Assuming a high enough barrier, ($V_0 \geq 30$), the interaction energy will make the energy gaps irrelevant. In this situation, the simplest picture is provided using the localized single particle basis, that is defined in Eq. (14). Using this basis, the Fock vectors can be written as, $\left|n_0^L, n_0^R, n_1^L, n_1^R\right\rangle_{\mathrm{lo}}$. So in our system, once the interaction is larger than the gap, the ground state is well

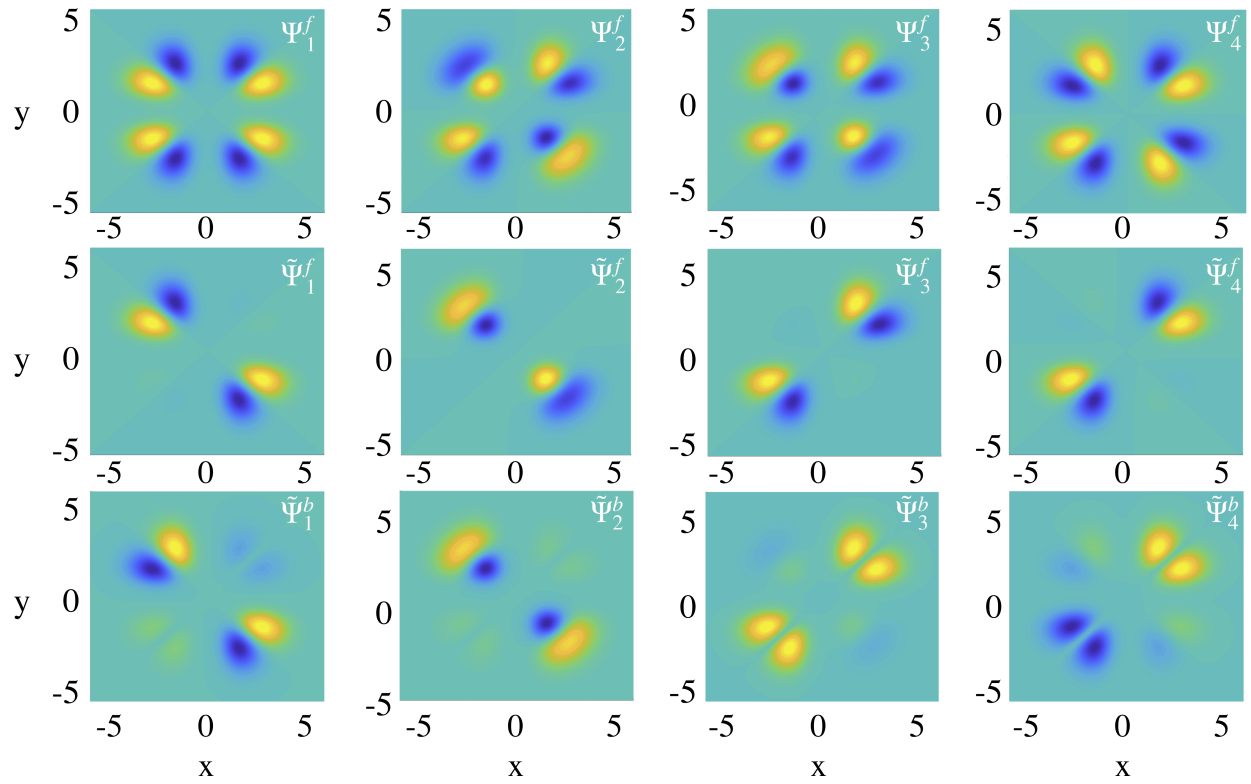

Figure 4: In the first row there are the first four fermionic excited states for $V_0 = 30$ calculated with the Slater determinants. In the second row there are the first four fermionic excited perturbed sates for $V_0 = 30$. In the third row there are the first four bosonic excited perturbed states for $V_0 = 0$. This results are obtained with the first quantization method.

approximated by $|1, 1, 0, 0, ...\rangle_{\text{lo}}$, this state has one atom in each well so the interactions do not affect it, we can see that in figure 3a. The first two excited states, quasi-degenerated with the ground state in the case of $g = 0$, this states are called the NOON states, $|\text{NOON}_2\rangle = \frac{1}{\sqrt{2}}(|0, 2, 0, 0..\rangle \pm |2, 0, 0, 0..\rangle)$, which contains a delocalized pair of interacting atoms, its energy increase when we increase the interactions (figure 3a). The next four excited states are also quasi-degenerated in the non-interacting case, one will remain constant with the interactions, $\frac{1}{\sqrt{2}}(|0, 1, 1, 0..\rangle \pm |1, 0, 0, 1..\rangle)$ and the other will increase again with the interactions, $\frac{1}{\sqrt{2}}(|0, 1, 0, 1..\rangle \pm |1, 0, 1, 0..\rangle)$, see figure 3a. Although all the studied results of this section are obtained with the first quantization method, we also obtain the same results with the second quantization method.

It is also worth to mention that in the fermion lines of figure 3a there is a slight dependence on g. Indeed, the dark blue and the maroon lines that start at $E \simeq 8.6$ increase their energies around $g \simeq 32$, in a way that we have avoided crossings with the purple boson line, this effect can be seen enlarged in figure 3b. We know that the Slater determinant, what we have used to define the fermion states, ensures that there are no interactions between the two particles. However, since we have not used a perfect delta contact potential, we can assume that our finite interaction potential induce a non-zero interaction between the two particles.

5. Quantum chaos

5.1. Level spacing distribution

Wave chaos consists in the study of wave motion when the geometrical limit of rays is chaotic, and that is what we detect in our classical system, the analogous for our two-particle system is quantum chaos [12]. There are different ways to detect quantum chaos in a system, the one used in this report is the same used in [11]. We will study the distribution of the spacing s between the neighboring unfolded specific levels. When there is no quantum chaos on the system, the distribution we expect is usually Poisson, $P_{\mathrm{P}}(s) = \exp(-s)$. This will happen in configuration with an excessive degeneration, so the space between a considerable number of levels will be zero, the distribution starts on the top. However, in chaotic configurations, crossings are avoided and the distribution will follow a Wigner-Dyson, $P_{\mathrm{WD}}(s) = \frac{s}{2}\exp\left(-\frac{\pi s^2}{2}\right)$. Comparing it with the previous situation, this time the distribution starts at zero, so it means that there is no degeneracy between the energy levels. Now we have to select the levels we want to use, in order to get a meaningful distribution the energy levels have to be separated by symmetry sector [16], so we will only use the bosonic states with positive parity. It will involve a different process for the first and the second quantization calculations. For the first quantization method, in order to only select the bosonic states we will check the symmetry around the contact interaction line $x_1 = x_2$ as we did before. Then, to just select the states with positive parity we will use the parity operator, that changes $x_1 \to -x_1$ and $x_2 \to -x_2$, so applying it to each state we can easily select the states with positive parity. The problem of this method is that we need to calculate all the states and then select the ones we want to use, so only a quarter part of the calculated states can be used in the study. For the second quantization method, we have to remember that we only have calculated the bosonic states thanks to the used commutation relations in section 3.1. In reference to the parity, we can apply the parity operator before the whole calculation. This method allows us to apply it directly to the basis Fock states with the equation $P = (-1)^{\sum_{j_{\mathrm{odd}}} n_j}$. This time, all the states we calculate can be used for the study, what will allow us to work with much more states.

5.2. Results

The aim of this section is to study the evidence we have found of wave/quantum chaos. The used bining for all the histograms in this section is the Rice rule, $b \simeq 2\, n_f^{1/3}$. In figure 5 we compare the level spacing distribution of our simulated system for different values of g, V_0 and σ_{dw}. On the one hand, for the first quantization method, we have calculated a total number of states $n_0 = 1300$, but with the restrictions we have explained in the previous section we will only can use around $n_f \simeq 330$ states for each histogram. We can see some results of these calculations in the first three rows of figure 5 [(a) to (i)]. On the other hand, for the second quantization method, we have calculated a total number of states $n_0 \simeq 1200$, what coincides with the number of states we can use, as we have explained before. We can see the results we get with this method in the last row of figure 5 [(j) to (l)].

In all the cases, when the interaction is small $g \sim 0$ the model is close to integrability, so the level spacing distribution is Poissonian, we can see this in the first column of figure 5. The same happens when the interaction is high; the magnitude of the coupling constant that causes again a Poisson distribution depend on the situation, we can see that in the third column of figure 5. Nonetheless, in the second column of figure 5 we see a different behaviour of our distribution, depending on the case it looks more like a Wigner-Dyson than a Poisson distribution. The clearest situation is the first one (b), that corresponds to $V_o = 10$, $\sigma_{\mathrm{dw}} = 0.5$, where we can conclude that we have quantum chaos. In the second one (e), we see that it looks more like a Poisson distribution, so we can conclude that the width of the double-well gaussian is very important to achieve quantum chaos. In the third situation (h), it is easy to see that there is quantum chaos again, so we have evidence that we can found quantum chaos for different values of V_0. In the last case (k) we can prove again that in the first situation we had quantum chaos, so this calculation is done with a different method but with the same parameters.

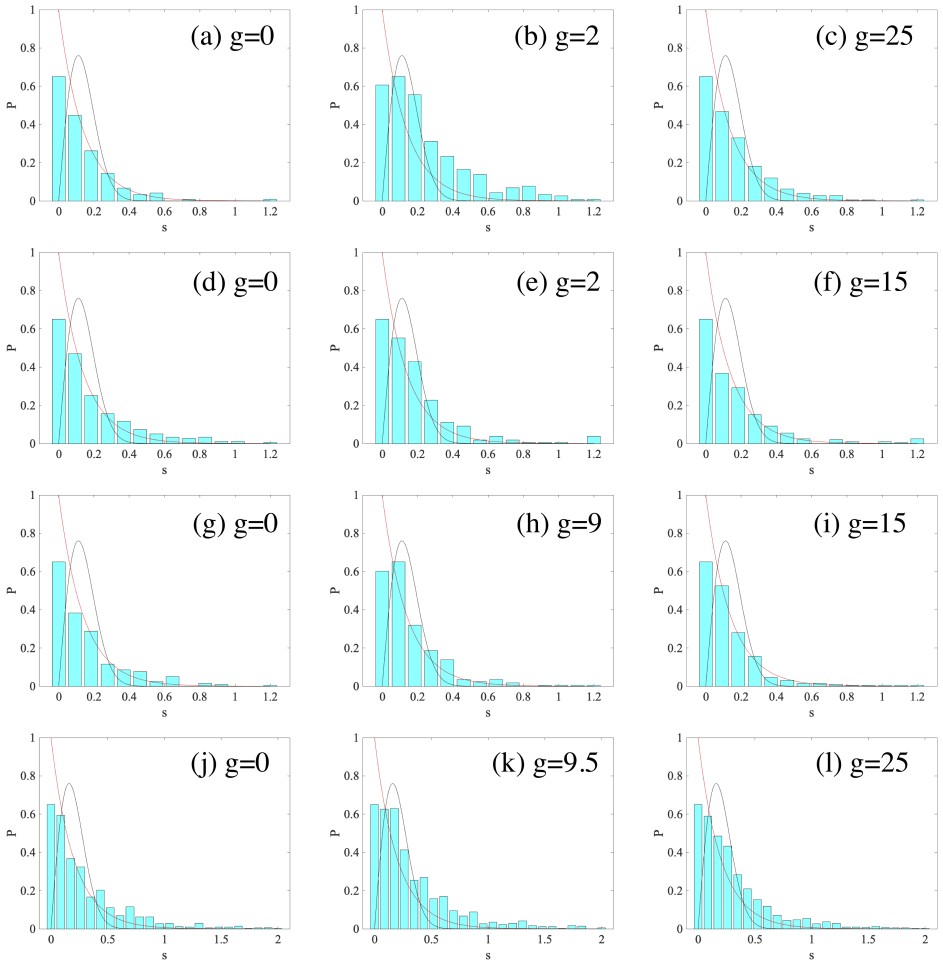

Figure 5: Normalized histograms of the energy level distribution. The red line is the Poission distribution, and the red line is the Wigner-Dyson distribution. The first three rows are calculated with the first quantization method, so we only get $N \simeq 300$. The first row correspond to the case of $V_o = 10$ and $\sigma_{\mathrm{dw}} = 0.5$, the second row correspond to the case of $V_o = 10$ and $\sigma_{\mathrm{dw}} = 0.05$ and the third row correspond to the case of $V_o = 20$ and $\sigma_{\mathrm{dw}} = 0.5$. Otherwise, the last row is calculated with the second quantization method, so we get $N \simeq 1200$, and it correspond the same situation as the first one but with the second quantization method.

6. Conclusions

We have shown that a quantum system consisting of two interacting atoms in one dimension can be simulated in an optical setup. To achieve this, we have introduced a new kind of optical fiber with a GRIN refractive index profile and three thin slabs of two different metallic materials. We have been able to relate the single particle solutions with the final energies and states of our quantum system. We have studied and characterized successfully the different states and energies of the system. Finally, we have provided evidence that we can have wave chaos in our system. We have been able to use second quantization, that is a quantum many body mathematical description, to describe what actually is an optics system. This represents an original method to perform numerics in the optics context.

References

[1] Wright L G *et al.* 2016 *Nature Photonics* **10** 771

[2] Longhi S 2009 *Laser & Photonics Reviews* **3** 243–261

[3] Harshman N L 2012 *Physical Review A* **86** 052122

[4] Girardeau M *et al.* 2001 *Physical Review A* **63** 033601

[5] Sowiński T and García-March M Á 2019 *arXiv preprint arXiv:1903.12189*

[6] Zinner N T *et al.* 2014 *EPL (Europhysics Letters)* **107** 60003

[7] García-March M *et al.* 2014 *Physical Review A* **90** 063605

[8] García-March M *et al.* 2015 *Physical Review A* **92** 033621

[9] D'Alessio L *et al.* 2016 *Advances in Physics* **65** 239–362

[10] Borgonovi F *et al.* 2016 *Physics Reports* **626** 1–58

[11] Garcia-March M *et al.* 2018 *New Journal of Physics* **20** 113039

[12] Doya V *et al.* 2002 *Physical Review E* **65** 056223

[13] Fedele R and Man'ko M 2003 *The European Physical Journal D-Atomic, Molecular, Optical and Plasma Physics* **27** 263–271

[14] Busch T *et al.* 1998 *Foundations of Physics* **28** 549–559

[15] Garcia-March M *et al.* 2019 *arXiv preprint arXiv:1902.01748*

[16] Santos L F 2009 *Journal of Mathematical Physics* **50** 095211